AWARD NUMBER: W81XWH-16-1-0017

TITLE: A 3D bioprinted model for the study of premalignant disease

PRINCIPAL INVESTIGATOR: Adrian V. Lee, PhD

CONTRACTING ORGANIZATION: University of Pittsburgh
Pittsburgh, PA 15260

REPORT DATE: MAY 2018

TYPE OF REPORT: Annual

PREPARED FOR: U.S. Army Medical Research and Materiel Command
Fort Detrick, Maryland 21702-5012

REPORT DOCUMENTATION PAGE

Form Approved
OMB No. 0704-0188

1. REPORT DATE	2. REPORT TYPE	3. DATES COVERED
May 2018	Annual	1May2017 - 30Apr2018

4. TITLE AND SUBTITLE

A 3D bioprinted model for the study of premalignant disease

5a. CONTRACT NUMBER

5b. GRANT NUMBER
W81XWH-16-1-0017

5c. PROGRAM ELEMENT NUMBER

6. AUTHOR(S)

Adrian V. Lee, PhD

Email: leeav@upmc.edu

5d. PROJECT NUMBER

5e. TASK NUMBER

5f. WORK UNIT NUMBER

7. PERFORMING ORGANIZATION NAME(S) AND ADDRESS(ES)

University of Pittsburgh
4200 Fifth Ave,
Pittsburgh,
PA 15260

8. PERFORMING ORGANIZATION REPORT NUMBER

9. SPONSORING / MONITORING AGENCY NAME(S) AND ADDRESS(ES)

U.S. Army Medical Research and Materiel Command
Fort Detrick, Maryland 21702-5012

10. SPONSOR/MONITOR'S ACRONYM(S)

11. SPONSOR/MONITOR'S REPORT NUMBER(S)

12. DISTRIBUTION / AVAILABILITY STATEMENT

Approved for Public Release; Distribution Unlimited

13. SUPPLEMENTARY NOTES

14. ABSTRACT

This proposal involves a multidisciplinary team including a surgical oncologist, a mammary gland biologist, a biomedical engineer, and a cancer biologist. We hypothesize that a novel in vitro 3D bioprinted model of premalignant breast cells growing within a breast ductal system will represent the first and most faithful representation of premalignant progression *in vitro* and will be an outstanding model for identify markers of low-risk premalignant disease which doesn't require treatment**.** In the yr 1 of the proposal we quantified mammary gland development, finding strain dependent differences highlighting a genetic component to development, and in yr 2 we continued to characterize development. In year 1 we developed a proof-of-principle 3D printing technology to print a mammary gland, and in year 2 we comprehensively developed a 3D printed ductal system with perfusion to study breast cells in their 3D environment. In yr 3 (NCE) we will examine growth and behavior of breast cells in this 3D mammary duct in vitro.

15. SUBJECT TERMS

None listed

16. SECURITY CLASSIFICATION OF:			17. LIMITATION OF ABSTRACT	18. NUMBER OF PAGES	19a. NAME OF RESPONSIBLE PERSON
a. REPORT	b. ABSTRACT	c. THIS PAGE			USAMRMC
Unclassified	Unclassified	Unclassified	Unclassified	15	19b. TELEPHONE NUMBER *(include area code)*

Standard Form 298 (Rev. 8-98)
Prescribed by ANSI Std. Z39.18

Table of Contents

1) Introduction

This proposal involves a multidisciplinary team including a surgical oncologist, a mammary gland biologist, a biomedical engineer, and a cancer biologist. **We hypothesize that a novel in vitro 3D bioprinted model of premalignant breast cells growing within a breast ductal system will represent the first and most faithful representation of premalignant progression *in vitro* and will be an outstanding model for identify markers of low-risk premalignant disease which doesn't require treatment.** In the yr 1 of the proposal we quantified mammary gland development, finding strain dependent differences highlighting a genetic component to development, and in yr 2 we continued to characterize development. In year 1 we developed a proof-of-principle 3D printing technology to print a mammary gland, and in year 2 we comprehensively developed a 3D printed ductal system with perfusion to study breast cells in their 3D environment. In yr 3 (NCE) we will examine growth and behavior of breast cells in this 3D mammary duct in vitro.

2) Keywords

DCIS, ductal cancer in situ, 3D bioprinting

3) Accomplishments

Regulatory approvals

In year 1, obtained IRB letter of exemption that the work is not human subjects research and IACUC approval for animal work at Baylor College of Medicine. We subsequently received HRPO/ACURO approval. All approvals were renewed in year 2.

Research progress

Major Task 1

Major Task 1 had 6 subtasks outlined for completion during year 1. Subtask 1 was completed during year 1 and reported in the first year annual report. Subtask 2 was partially completed during year 1 and has been essentially completed now in year 2 (detailed below). Subtask 3 is about 75% completed now at the end of year two and will be completed during the NCE.

Subtask 1: Purchase and breed mating pairs for 12 strains of mice from which to isolate mammary tissue wholemounts for 3D imaging from virgin females at 2 developmental ages. This task was completed in year 1 (see progress report for that year).

Subtask 2: Whole mount mammary glands (60) from PN17 mice, stain with luminal and myoepithelial markers, and capture tomography data at the OIVM core. This subtask was to be completed during months 4-8. This subtask consisted of whole mounting mammary glands (60) from post-natal day 17 (PN17) mice, stain with luminal and myoepithelial markers, and capture tomography data at the OIVM core. Examples of stained samples were shown in the year 1 progress report. This age of mouse was chosen because it represents an age just prior to the onset of puberty where the development of the gland is relatively simple and not yet under the dominating influence of estrus cycles. This subtask is essentially completed. Of the 12 strains that were targeted for analysis at PN17, there was only one, CAST/EiJ, that we could not get samples from. The reduced fecundity of this strain was identified as a problem in year 1.

Although we brought in several batches of breeding pairs from the Jackson lab in order to establish a productive colony CAST/EiJ this effort was unsuccessful.

Subtask 3 Segment, annotate, and measure 3D reconstructions obtained in Subtask 2. Send the annotated 3D rendering data to Pittsburg for 3D printing. This subtask was to be completed during months 4-8 and consisted of segmentation, annotation, and measurement of the ductal trees in 3D reconstructions obtained in Subtask 2. This subtask was about 50% completed by the end of year 1 and is now essentially completed. To date, 11 of 12 planned strains have been analyzed for 8 of the 10 measurements that were planned and the last 2 measurements, inclusion and discordance, should be completed on these within a few weeks. We are also continuing to send reconstruction data from PN17 samples to the University of Pittsburg for 3D printing. A summary of the data from 5 of the completed strains was presented in a poster during year 1 at the 2017 Experimental Biology Meetings in Chicago IL. This work represented the first 3D comparison of ductal architecture and patterning in inbred mouse strains of different genetic backgrounds. The hypothesis for the study was that ductal patterning, and the implementation of stereotypical branching behaviors during early post-natal development differs with genetic background. As described in the year 1 progress report a software package called TreeSurveyor (Short and coworkers, 2013) was used to identify, annotate, and measure all of the ductal segments and branch points in each reconstructed tree (see year 1 progress report).

Comparisons of overall ductal geometry among the 11 completed strains revealed that genetic background had significant ($P<0.05$) effects on all but two of the traits that were measured. Figure 1 shows the effects of genetic background on overall mammary ductal geometry. Differences were evident in total duct length (Figure 1A), average duct length (Figure 1B), total branch count (Figure 1C), and branch density (Figure 1D), as well as in ductal segment diameter (Figure 1E) and curvature (Figure 1F). With regard to total ductal length (Figure 1A), there was about a 2.5-fold difference ($P<0.05$) between strains at the top (C57BL/6J, CZECHII/EiJ and PWK/PhJ) and bottom (A/J, WSB/EiJ, NOD/LtJ) ends of the distribution. This difference was primarily driven by the fact that these same strains displayed similar differences in the average ductal segment length (Figure 1B). For some strains, such as CZECHII/EiJ, total branch count (Figure 1C) may have also contributed somewhat to overall length of the ductal tree. In this regard, there were also strains such as 129S1/SvImJ and Bub/BnJ that had high total branch counts, but short duct length, which resulted in high overall branch density (Figure 1D). Overall ductal diameter (Figure 1E) was highest in PWK/PhJ and CZECHII/EiJ, however, there were two strains, C57BL6J and KK/HlJ, that displayed high levels of intra-strain variation for this trait. Ductal curvature (Figure 1F) was highest for BUB/BnJ and WSB/EiJ, which were also strains that displayed the highest branch density overall. Neither bifurcation angle (Figure 1G) nor dihedral angle (Figure 1H) were influenced by genetic background. The overall mean for bifurcation angle was 96.9±5.0 degrees and ranged from a high of 101 ± 5^{o} in NOD/LtJ to a low of 93 ± 2^{o} in PWK/PhJ suggesting the in general bifurcation events during branching morphogenesis tend to be right angles. For dihedral angle the overall mean was 76.5±6.9 degrees with a high of 79 ± 3^{o} in NOD/LtJ and a low of 74±3 in KK/HlJ implying that in general branching events during ductal morphogenesis in the mammary gland are orthogonal with respect to rotation.

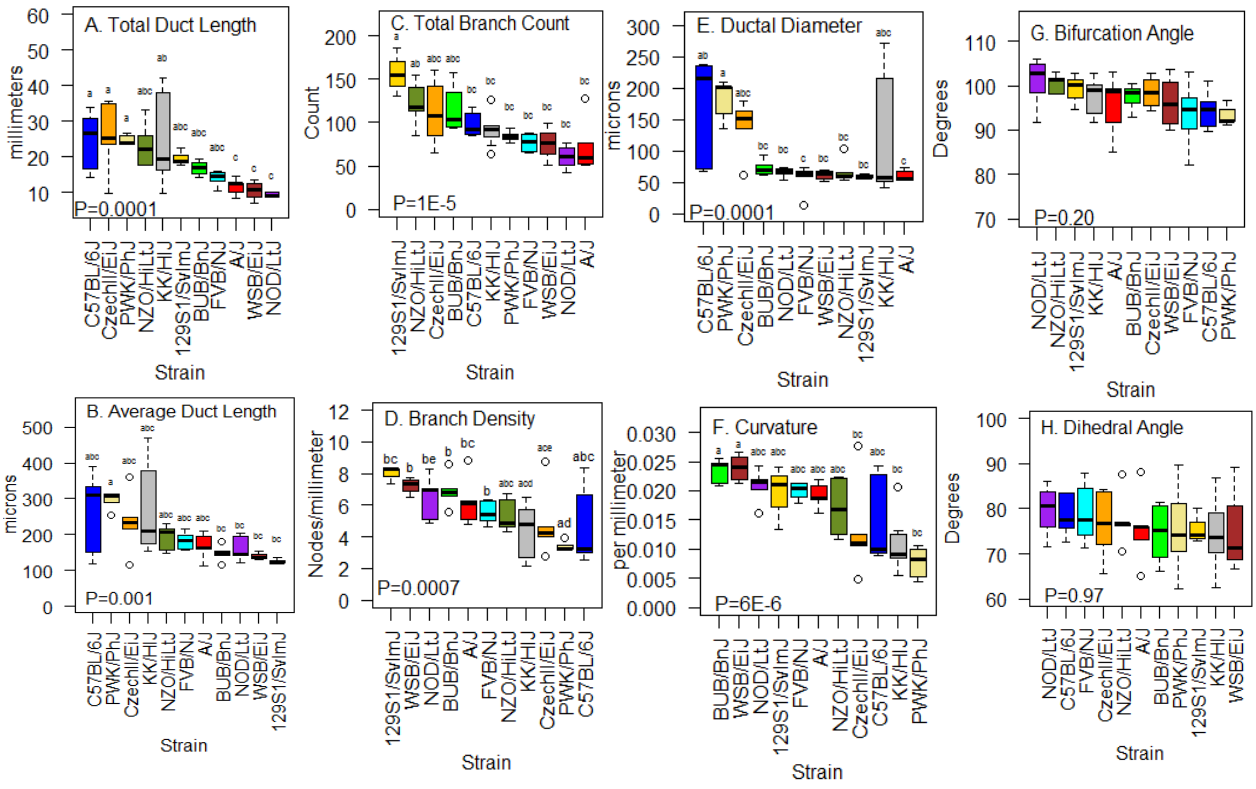

Figure 1. Genetic Background influences overall mammary ductal geometry. Three-dimensional reconstructions were prepared from E-cadherin-stained mammary whole mounts. Tissues were collected from females of 11 different inbred strains at post-natal day 17 of age. Shown are (A) total duct length, (B) average duct length, (C) total branch count, (D) branch density, (E) ductal diameter, (F) curvature, (G) bifurcation angle, and (H) dihedral angle. Each box represents the data for 3 to 7 animals. Statistical significance was set at α=0.05. Boxes are ordered by strain median. Boxes with similar superscripts are similar (P>0.05) by Tukey's HSD.

Analysis of regional variation within the ductal trees at PN17 was also accomplished in all 11 strains. The results of this regional analysis are shown in Figure 2. A significant effect of generation was detected for branch count (Figure 2A), length (Figure 2B) diameter (Figure 2C), and curvature (Figure 2D). For branch count (Figure 2A), all 11 strains exhibited a continuous increase for at least the first 6 generations. However, by generation 5 the strains started to differentiate themselves. For some, like NZO/LtJ and 129S1SvImJ, branch counts continued to increase through the next 5 to 7 generations and then dropped off in later generations. Others like NOD/LtJ, WSB/EiJ and A/J, added branches at a slower rate. For all 11 strains average duct length (Figure 2B) was highest in the root (generation 0) and first generation branches and decreased with branch generation. The exception observed in branch length was with KK/HlJ, which appeared to have increase in branch length in later generation. This increase, however, was only observed in a single animal. Branch diameter (Figure 2C) similarly started out highest in the early generations and gradually decreased with progression toward later generations. In this regard there were 4 strains C57BL/6J, PWK/PhJ, CZECHII/EiJ, and KK/HlJ that exhibited much larger branch diameters than the remaining strains. Differences were also observed in branch curvature among certain strains with progression through ductal tree (Figure 2D). In

general, among the strains that exhibited generation-dependent variation, curvature tended to be highest in earlier generations. Neither bifurcation angle (Figure 2E) nor dihedral angle (Figure 2F) changed significantly with generation. In this regard, an inability to observe changes could possibly be attributed to the fact that both internal and terminal branches both contribute to these two measurements. We are currently in the process of classifying the branches based on their relative location within the ductal tree. The TreeSurveyor package has an option that will allow for stratification of individual branches on the basis of whether they are internal or terminal. This should allow us to determine with greater selectively, if branch angles and even the other traits discussed are affected by whether they are internal or terminal structures. These results support the preliminary conclusion that genetic background, acting through sequence variants at specific genomic loci, can influence ductal diameter, length, and curvature.

The last set of traits to be compared among PN17 samples describe the degree of conservation between the ductal structures within any given strain. A preliminary report on these traits based on 5 strains was made in the year 1 progress report. The analysis of these traits is ongoing and will be completed during the no-cost extension.

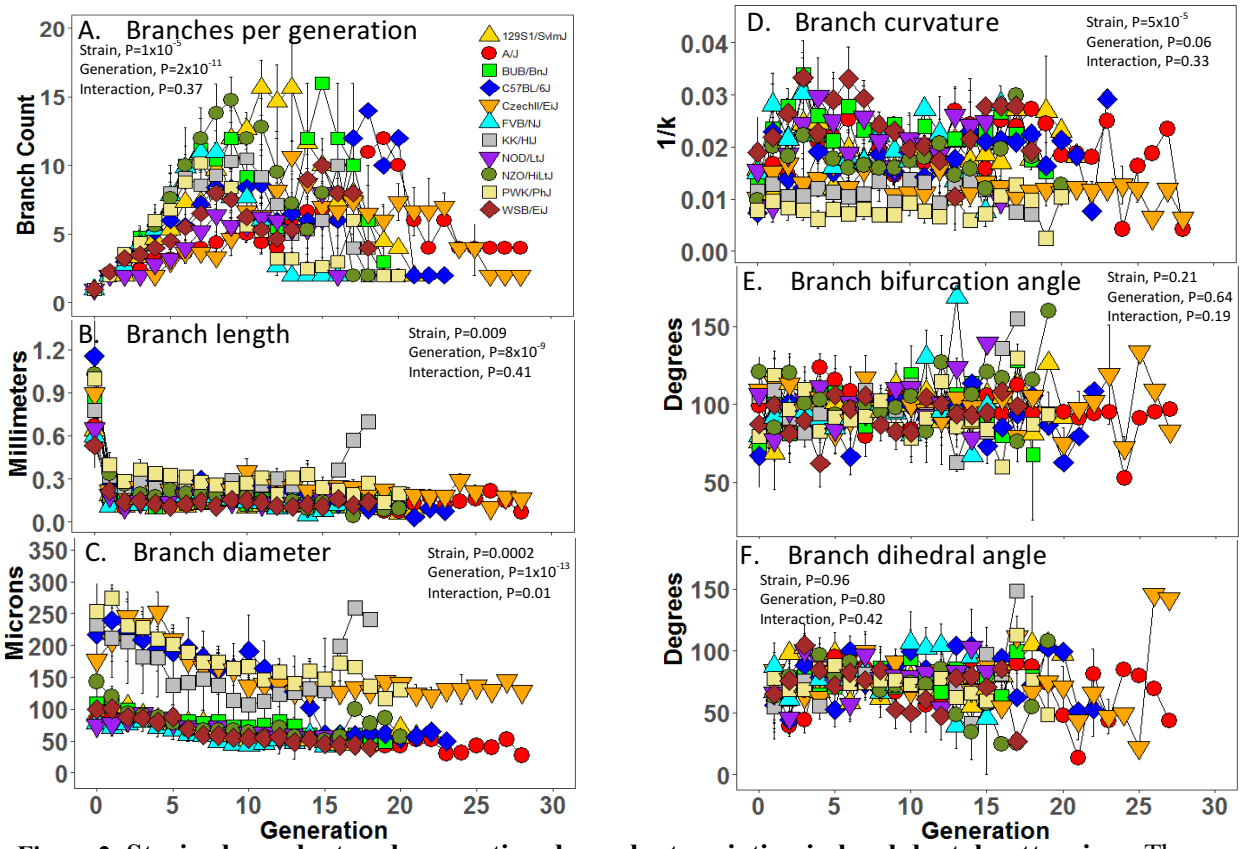

Figure 2. Strain-dependent and generation dependent variation in local ductal patterning. Three-dimensional reconstructions were prepared from E-cadherin-stained mammary wholemounts. Tissues were collected from females of 11 different inbred strains at post-natal day 17 of age. Shown are (A) branch count, (B) branch length, (C) branch segment diameter, (D) branch curvature, (E) bifurcation angle, and (F) dihedral angle. Each symbol represents the mean±s.e.m. for 3 to 7 animals. Statistical significance was set at α=0.05.

Subtask 4 Whole mount mammary glands (30) from PN64 mice, stain with luminal and myoepithelial markers, and capture tomography data at the SANTA core. This sub-task was to be completed during months 6 – 9 and involved whole mount staining mammary glands (60) from PN64 mice for the same luminal and myoepithelial markers used on the PN17 mice. Although we continue to work on this subtask, our progress has been slow. The main reason for this comes from the fact that with limited resources to support a larger breeding colony and the personnel to carry out the studies we felt that it was most efficacious to complete the PN17 data prior to moving on to a full focus on the PN64 animals. Now that the PN17 animals are essentially finished, we are turning our focus towards completion of the PN64 samples. To date we have collected at least 1 sample from all but two of the proposed strains (Table 1). In addition, during the course of identifying prospective mice for sampling, all of the females within the breeding colonies for the 11 strains studied were observed for the timing of sexual maturation, as indicated by vaginal patency. The results of this analysis are shown in figure 3. Genetic background has a dramatic effect ($P=2x10^{-16}$) on the timing of sexual maturation. This fact is a very important consideration to the interpretation of data from the PN64 samples. In particular wild-derived strains such as CZECHII/EiJ, PWK/PhJ, and WSB/EiJ can undergo sexual maturation up to two weeks later that some of the classical strains such as BUB/BnJ. The collection and analysis of the remaing PN64 samples will be completed during the no-cost extension and a manuscript describing the impact of genetic background on pre and post-pubertal ductal patterning in the mouse will be published.

Table 1. Progress on PN64 sample processing

STRAIN	Usable samples processed
129S1	5
A/J	1
BUB/BnJ	0
C57BL6/J	5+
CAST/EiJ	0
CZECHII/EiJ	3
FVB/NJ	2
KK/HlJ	5+
NOD/ShILtJ	1
NZO/HltJ	0
PWK/PhJ	2
WSB/EiJ	2

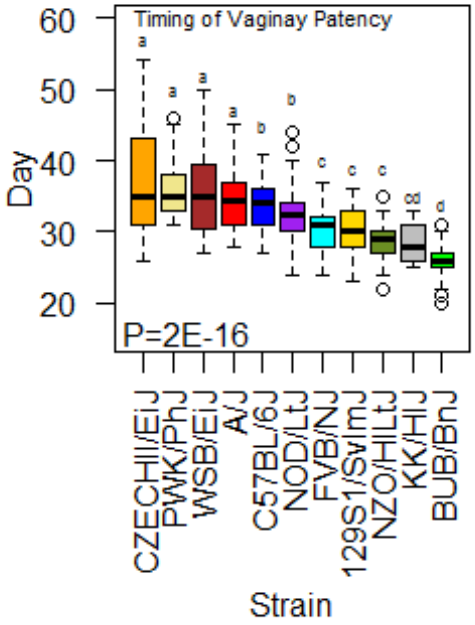

Figure 3. Timing of Vaginal Patency. Vaginal patency was detected visually in cohorts of prospective study females beginning with weaning at post-natal day 21. Each bar represents the data for from 20 to 122 females that were visually observed twice weekly until observation of vaginal opening. Bars with similar superscripts are similar (P>0.05) by Tukey's HSD.

Subtask 5: Purchase lactating dams with litters (2 each) for each of 3 rat strains. The strains will be ACI/Seg/Hsd from Harlan Laboratories, and Sprague-Dawley and Wistar, both from Charles River Laboratories. There will be 5 females studied at PN64 for each of the 3 strains. This sub-task was to be completed during months 8 through 9. Because of size limitations in the imaging instruments and an inability to get enzyme-

metallography to work. We will not attempt any further work on this subtask.

Subtask 6: Whole mount mammary glands (15) from PN64 rats, stain with luminal and myoepithelial markers, and capture tomography and Micro-CT data at the OIVM core. After several attempts at staining these larger samples for enzyme metallography we concluded that this subtask was infeasible and will not attempt any further work on this.

Major Task 2

Major Task 2 had 4 subtasks outlined for completion during year 1, and 2 subtasks to be initiated during year 1 and extending into year 2. Although not all of these have been completed to date, 3 substasks are completed and the rest are on track to be completed soon.

Task 2 Subtask 1 (completed Year 1) was to be completed during months 4 through 12 and was to 3D print mammary ductal structure images using ECM hydrogels. As noted in the year 1 annual report, this subtask has been completed and we have fully developed and implemented this capability. To do this we implemented a new 3D bioprinting approach that allowed us to directly print with collagen type I and additional ECM protein hydrogels while achieving high fidelity and resolution better than 100 μm.

Task 2 Subtask 2 (completed Year 1) was to be completed during months 6-12 and consisted of tomography imaging and evaluation of 3D printed mammary ductal structure, with one sample to be evaluated. We made significant progress on this goal, and completed it per the initial target milestones (see year 1 report). We 3D printed a 200% scale ductal trees from collagen type I. The files used to generate these trees were obtained from Co-investigator Dr. Hadsell and processed through several iterations of workflow that eventually resulted in a continuous, manifold mesh without visible tiling artifacts, stacking artifacts, or floating solids. The file was scaled to 200% to allow the printer to deposit a significant portion of the construct using a filamentous extrusion rather than as punctate depositions. Slower machine movements along with denser alginate mesh improved print quality substantially. The mammary duct model we developed represents a world-first level of complexity generated using a bioprinter with multiple ECM and hydrogel components (see year 1 report).

Task 2 Subtask 3 (completed Year 2) was to be completed during months 8-12 and consisted of 3D printing the mammary ductal structure using progenitor cells (HMEC, MCF10A, HS578BSt).

As described in the year 1 report, to avoid the challenges of perfusion seeding and still enable distribution of cells throughout a construct with a sealed lumen, it was decided to try and seed constructs using a gravity-driven fluidic distribution system included in the mammary construct geometry. Mammary constructs had the same fundamental collagen component design of a funnel that fed into a tube “duct” which terminated in a spherical “bud”. It was assumed that the funnel could be held up above the surface of cell culture media and used as a receptacle for a cell suspension and allow cell suspension to flow down into the rest of the construct through the walls of the duct and bud. It was hypothesized that, were it not possible to seed the sides of the duct and bud using this approach, then the construct could be seeded in waves, and the construct could be rested on its side to allow for each wave of cells in to coat the sides of the duct and bud.

To allow for introduction of the cell suspension to the funnel and for resting of the construct on its side, the alginate mesh reinforcement was designed as a cube centered on and surrounding the collagen component.

Task 2 Subtask 4 was to be completed during months 10-14 and involved tomography imaging and evaluation of 3D progenitor cell-printed mammary ductal structure. This work was initiated and is ongoing.

A concern we realized from the construct from **Subtask 3** above was that the cells compacted the collagen and caused a loss of structure. In all cases, constructs showed some degree of delamination between the alginate and collagen sections of the constructs visible at the rim of the funnel (Figure 4), regardless of cell type used. It was thought that this disconnection was the result of the collagen-alginate connection being particularly weak at the rim of the funnel. This produced inconsistent growth and inhibited complete characterization.

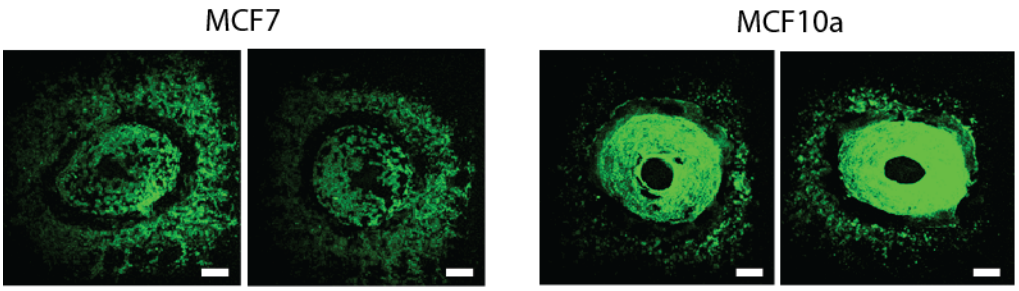

Figure 4. Delamination of collagen is consistent across constructs seeded and cultured for a week. Constructs shown on the left were cultured with MCF7 cells, and constructs on the left were cultured with MCF10a cells. In all constructs, a gap of cells was visible around the top rim of collagen, indicating that the collagen was originally there but pulled away under the action of cells. Otherwise, we would expect to see cells scattered around the edge of the rim on all regions of top-side alginate. Scale bars are 1 mm.

Task 3 was to be completed during months 12-18 and involved injecting cells into printed mammary ducts and monitoring growth and progression.

We encountered significant challenges during Task 3 in Year 2 because the 3D printed mammary duct developed in Task 2 Subtask 3 (Fig 4) showed delamination of collagen and inconsistent seeding of cells within the ductal structure. To ensure reproducible growth and quantification, we instituted a re-design of the printed construct and the bioreactor platform to support growth and culture of the construct.

Task 3 Subtask 1 was to be completed during months 12-16 and involved fluorescently labeling DCIS cells and injecting into 3D printed ductal system and monitoring using microscopy. As shown in Fig 4, the initial results placing cells in this device were not conducive to growth and measurement. We therefore set about redesigning the printed construct and the bioreactor platform to support growth and culture of the construct. This is described below and is complete and cells are currently being injected and will be studied in yr 3 (during a no cost extension)

We decided to redesign the platform and include a bioreactor system that would enable controlled fluid flow for cell seeding coupled with controlled fluid flow throughout the culture process to ensure proper nutrient supply and waste removal.

In Figure 5 we show the redesigned mammary duct tube designed and constructed in Year 2 and planned to be used in Tasks 3-5 to be completed in year 3 during the no cost extension. This new system is printed entirely in collagen type I and has an inner diameter of 1.4 mm, to match a nominal size in the human breast (Figure 5A). We have achieved highly repeatable 3D printing using our FRESH technique and have produced >25 of these constructs with no issues and extremely high fidelity (Figure 5 B and C). We have validated that the tube that serves as the mammary duct is manifold and performed perfusion studies that have shown low permeability using various molecular weight dextran solutions, to simulate biological molecules.

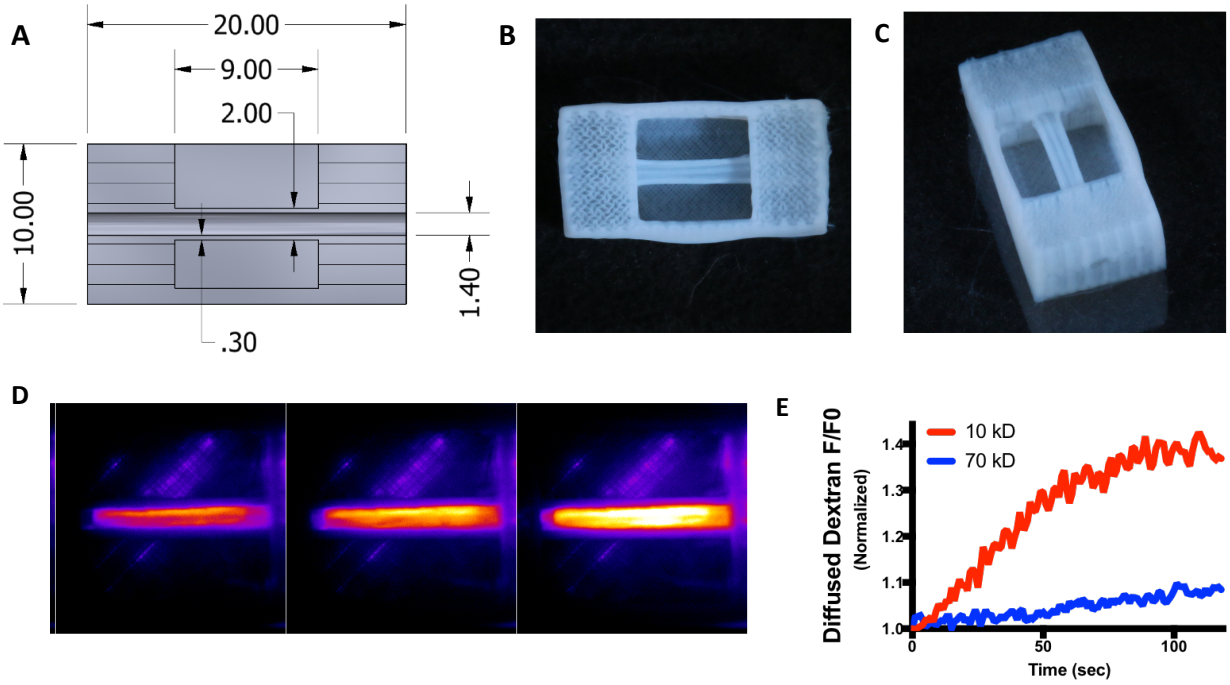

Figure 5. The redesigned mammary duct construct showing the simplified tube design and perfusion validation. (A) Schematic of the construct. (B and C) Photographs of the construct printed entirely from collagen type I using the FRESH 3D bioprinting method. (D) Perfusion studies using our bioreactor platform to perfuse fluorescent Dextran of various molecular weights through the lumen and tracking diffusion through the tube wall. (E) Quantification of the perfusion and permeability studies in (D), showing as expected that diffusion through the wall depends on molecular weight, but also that there are no large defects.

In Figure 6 we show that this redesigned mammary construct also enables straightforward engineering of stromal tissue around the mammary duct tube by casting a collagen gel with embedded cells. The previous duct and end bud construct developed in Task 2 in year 1 enabled luminal seeding, but the surrounding alginate support prevent creation of stromal-like tissue. Here the empty region around the tube can be filled with a collagen gel with embedded stromal

cells (Figure 6 A). We then culture this as normal and show that the stromal tissue around the tube can contain viable cells (Figure 6 B).

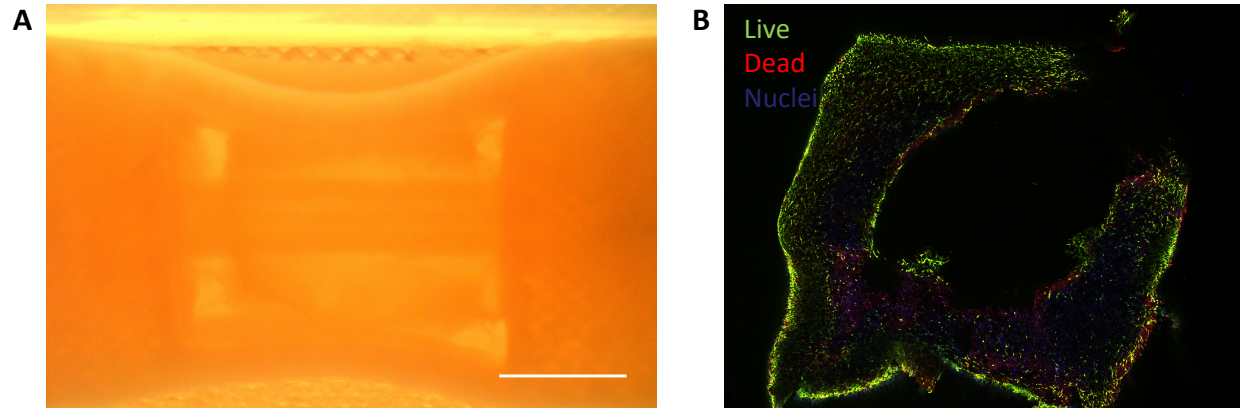

Figure 6. Example of the redesigned mammary construct with the addition of stromal-like tissue around the ductal tube in the center of the construct. (A) A brightfield image of the construct inside the bioreactor perfusion system with a collagen gel with embedded cells cast around the central tube region. (B) A cross-section of the tube construct that has been sectioned and stained with LIVE/DEAD showing uniform cell distribution throughout shortly after fabricating the entire construct.

In Figure 7 we validate the importance of having the ductal tube within the center of the stromal tissue construct. We show that with on the ductal tube to provide mass transport of nutrients and waste, that cells in the bulk of the stromal tissue rapidly die. This is a function of depth from the surface of the construct.

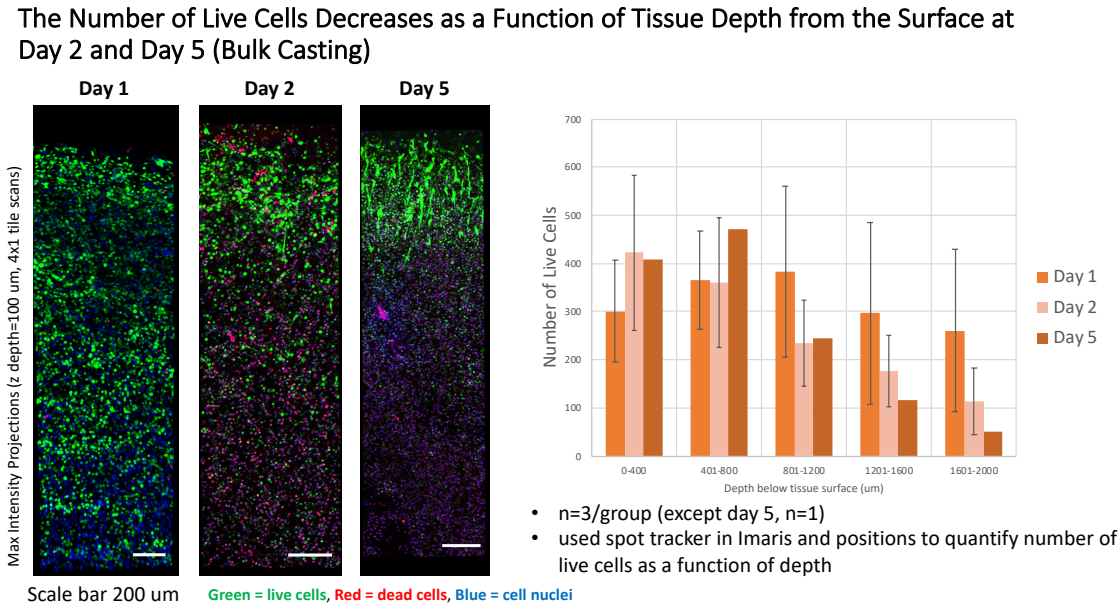

Figure 7. Example of the stromal tissue showing that without the mammary ductal tube, that the cells quickly die in the construct. (Left) Example images showing the decrease in live

cells (GREEN) in the stromal tissue when there is no ductal tube. (Right) Quantification of cell viability as a function of time and depth within the stromal tissue construct that lacks the ductal tube in the center.

In Figure 8 we show that the presence of the ductal tube in the construct is critical to the performance. When we culture the construct with the mammary ductal tube in the center and the stromal tissue around the tube for 5 days in statist culture, the results end up being very similar to the construct without the tube as shown in Figure III. Basically, under static conditions the only viable cells are on the top surface of the construct where the media is located. In contrast, when perfusing the lumen of the tube a low rates to simulate luminal fluid flow we are able to maintained high viability throughout the construct with highly spread and active cells.

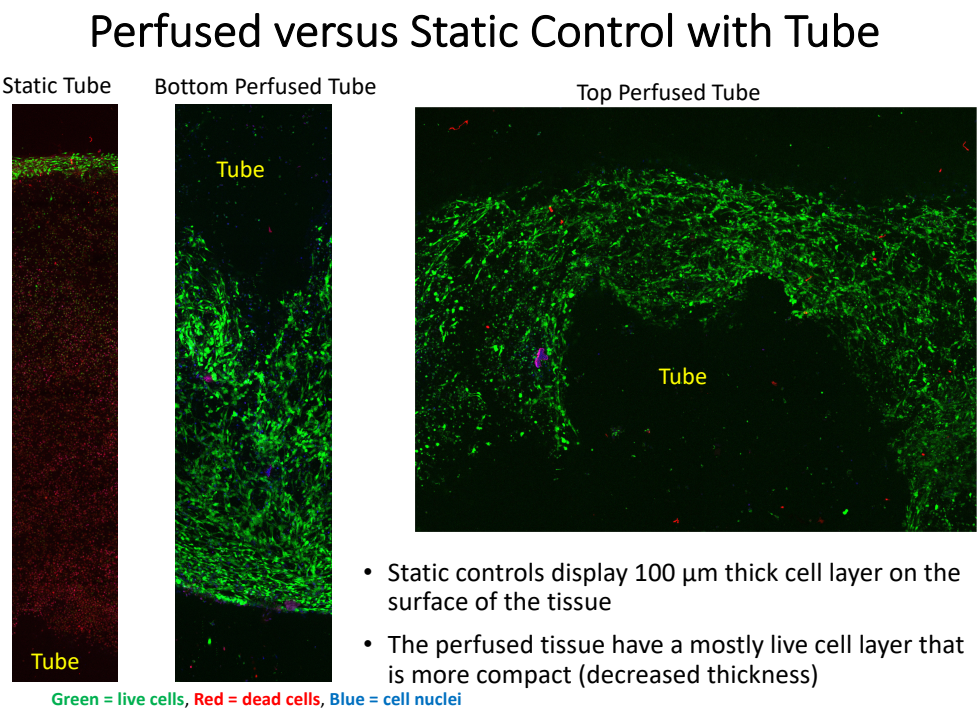

Figure 8. Examples of static and perfused constructs with the ductal tube showing that perfusion is critical for forming volumetric stromal-like tissue around the tube. (Left) The static tube after 5 days in culture has a layer of LIVE cells at the top where the media is but otherwise cells within the construct have died. (Center and Right) In contrast, after 5 days the perfused construct shows high viability throughout the stromal portion of the construct and on both the top and bottom sides of the tube.

Now that we have a functional construct we are in the process of completing Task 3 and all of the subtasks.

Task 4 focused on RNA-seq analysis of premalignant progression. Experimental **Subtasks 1-3** were to be completed during months 14-22 and involved (i) growing DCIS cells in 3D printed duct and harvest after 2 weeks and once invading (predicted 4 weeks), (ii) FACS sorting

ZsGreen positive premalignant cells and isolating RNA, and (iii) performing RNA-seq and bioinformatics analysis.

This task has not been started because of the challenges encountered during Task 3 to engineer a model of the mammary duct that provided acceptable ability to achieve and monitor growth. The purpose of the No Cost Extension, which has been approved, is to complete Task 4. We are on track to do this, having already placed cells within the ductal system and are in the process of completing experiments.

Task 5 focused on Functional screen for genes important in progression and experimental **Subtasks 1 and 2** were to be completed during months 18-24 and involved taking premalignant cells infected with a lentiviral cDNA ORF or shRNA (and control) against five candidate genes from Task 4 and then injecting these cells into 3D printed ducts and monitor growth and progression and compare to control infected cells. This was to be followed by evaluation of the 3D patterning of up to 2 select cultures by OPT.

This task has not been started because we are waiting for results from Task 4, which is ongoing. The purpose of the No Cost Extension, which has been approved, is to complete Task 5. We are on track to do this, having already developed or in the process of completing technologies and experiments to do so.

4) Impact

Our data thus far indicate that different strains of mice exhibit different mammary gland structures, suggesting a genetic component to development. Having a comprehensive quantification of mammary gland development may yield insight into risk factors for subsequent development of breast cancer. This work is close to finished and will be submitted for publication. We expect this work to be of great interest to those in the field of mammary gland biology and breast cancer.

3D printing of mammary glands is progressing. An initial design for 3D printing of a simplified tube was successful however cells didn't seed reproducibly and we noted delamination of collagen in the ductal tube. This system was not suitable for quantitative measurement of breast cell growth and invasion in a 3D ductal environment. We therefore re-designed the ductal system and now have an advanced design that allows perfusion and shows better growth patterns. We are now using this system to study the growth of breast cells in a 3D microenvironment.

5) Changes/problems

In year 1 we encountered minor difficulties such as reduced fecundity in some mouse strains, but we continued these studies in year 2 and complete the mammary ductal development studies as noted above. During year 2, we had to change the design of the 3D ductal microenvironment, as the method we developed at the end of year 1 showed uneven plating of cells and delamination of collagen. We re-engineered the 3D ductal environment to allow perfusion and easier plating of cells. Preliminary results show that this model has better cell plating and cell survive when toxins are removed by perfusion. In year 3 (NCE) we will now study growth of cells in this microenvironment.

6) Products
Whole mounts of murine mammary glands
Images and reconstructions of mammary glands
3D printed tubes with perfusion representing ducts

7) Participants and other collaborating organizations
Darryl Hadsell PhD, Baylor College of Medicine (subcontract to Partnering PI)
Adam Feinberg, PhD, Carnegie Mellon University (Partnering PI)
Priscilla McAuliffe MD, PhD University of Pittsburgh (Partnering Co-Investigator)

8) Special reporting requirements
None

9) Appendices
None